was released into the laboratory air at the start of the experiment. For the next ½ hour fresh samples of room air were introduced into the apparatus at 2-minute intervals, and absorption at the P(14) line (10.5321 μm) of the CO_2 laser was measured. The background signal was subtracted from the measured signals, which were then converted into equivalent gas concentrations. The gas concentration decreased rapidly because of the forced ventilation of the laboratory. The ethylene concentration, which was initially 2000 ppb, fell to 5 ppb in approximately ½ hour. A plot of the logarithm of the concentration as a function of time (Fig. 1B) yields a straight line, with a scatter of less than 1 ppb in the data points at low concentrations. Thus, the detection sensitivity for ethylene calculated from calibration measurements at high concentrations could be realized at low concentrations.

In most air pollution measurements the sample contains more than one gas that absorbs in the infrared. It is not usually possible to find a wavelength that is absorbed by the component of interest and not by any other component. Thus, the problem of interference will be present and must be overcome. The concept of a rejection ratio is useful for evaluating interferences. Suppose that it is desired to detect a gas A and that this measurement is interfered with by a gas B. Then there will be some concentration C(B) of gas B that just prevents the unambiguous detection of a concentration C(A) of gas A. The rejection ratio is defined as $C(\mathrm{B})/C(\mathrm{A})$. Its size depends on the relative absorption strengths of the two gases and on the precision with which their concentrations may be measured. With our present apparatus we can measure concentrations with an accuracy of 0.1 percent. This gives a rejection ratio equal to 10^3 times the absorption strength of gas A divided by the absorption strength of gas B, measured at the wavelength used to detect gas A. It is assumed that there is another wavelength where the concentration of gas B may be measured. Care must be taken to control the sample temperature since different gases have different temperature dependences for absorption.

Rejection ratios for the gases listed in Table 1 have been calculated from measured absorption strengths by using the experimentally achieved measurement accuracy of 0.1 percent. The most severe problem occurs between NO and water vapor. Since NO is a diatomic molecule it has only one strong infrared absorption band, which is centered at about 5.3 μm and is overlapped by strong H_2O absorption bands. In practice, it is often necessary to detect small concentrations of NO in the presence of large water vapor concentrations. Automobile exhaust may contain as much as 10 percent water vapor, and measurements of ambient air are required up to 120°F and 100 percent relative humidity. If NO is measured at the CO laser emission wavelengths of 5.2640 and 5.3080 μm and water vapor is detected at 5.8292 and 5.9417 μm, the rejection ratio is 10^6. That is, for sources with 10 percent (10^5 ppm) water vapor the detection limit for NO is 0.1 ppm, and for ambient air at 120°F and 100 percent relative humidity the limit is 0.01 ppm. Nitrogen dioxide detection is also interfered with by water vapor. If CO laser transitions at 6.2272 and 6.2552 μm are used, the rejection ratio is 10^7. Thus, NO_2 concentrations of 0.01 ppm should be detectable in automobile exhaust, and concentrations of 1 ppb should be detectable in ambient air. Typical uncontrolled automobile exhaust contains NO and NO_2 in concentrations of 100 to 1000 ppm (*7*), and ambient urban air in most cities has NO and NO_2 in concentrations of 0.01 ppm or more 99 percent of the time (*8*). Thus, the above sensitivities should be adequate for this type of measurement.

The rejection ratios between all pairs of gases in Table 1 exceed 10^4. This rejection ratio, combined with the sensitivities listed in Table 1, provides a measure of the practical utility of this technique. Not all gaseous air pollutants absorb in the emission range of the lasers used in this experiment. However, many different laser transitions have been demonstrated in the infrared (*9*). It should be possible to find appropriate transitions for most pollutants and to achieve rejection ratios large enough so that samples of mixed gases can be analyzed.

L. B. KREUZER
N. D. KENYON*
C. K. N. PATEL
*Bell Telephone Laboratories, Inc.
Murray Hill, New Jersey 07974*

References and Notes

1. The use of gas lasers for pollution detection has been discussed by: R. T. Menzies, *Appl. Opt.* **7**, 1532 (1971); ———, N. George, M. K. Bhaumik, IEEE *J. Quantum Electron.* **6**, 800 (1970); P. L. Hanst, *Appl. Spectrosc.* **24**, 161 (1970).
2. L. B. Kreuzer, *J. Appl. Phys.* **42**, 2934 (1971).
3. ——— and C. K. N. Patel, *Science* **173**, 45 (1971).
4. C. K. N. Patel, *Phys. Rev.* **141**, 71 (1966).
5. ———, P. K. Tien, J. H. McFee, *Appl. Phys. Lett.* **7**, 290 (1965).
6. C. Freed, *ibid.* **18**, 458 (1971).
7. A. C. Stern, *Air Pollution* (Academic Press, New York, 1968), vol. 1, p. 40.
8. ———, *ibid.*, vol. 3, pp. 60–61.
9. R. J. Pressley, *CRC Handbook of Lasers*, M. L. Wu, Ed. (Chemical Rubber, Cleveland, 1971), pp. 298–349.

* Present address: Post Office Research Station, Martlesham Heath, Ipswich Suffolk, England.

5 April 1972; revised 22 May 1972

Second-Order Scattering from the Sea: Ten-Meter Radar Observations of the Doppler Continuum

Abstract. *Ten-meter radar observations of the sea have been used to study second-order interactions between waves in electromagnetic scattering from the sea. Techniques of coherent, pulsed radar provide echo frequency spectra from several range intervals. The echo spectra are resolved with an analysis window of a few millihertz. These spectra show a clear second-order echo continuum which appears as sidebands about the first-order Bragg scattering lines. Up to one-half of the total echo power has been observed in these sidebands. The principal characteristics of these sidebands vary with time, apparently in response to the sea state. The form of the echo spectra is consistent with the results of perturbation theory computations based on Rice's method.*

Bragg scattering is generally accepted as the principal scattering mechanism responsible for medium-frequency and high-frequency radar returns from the sea. As first suggested by Crombie (*1*), electromagnetic waves of length λ_e are backscattered from ocean waves of one-half that length, $\lambda_e/2$. According to this hypothesis, the radar echo frequency is shifted because of the movement of the ocean waves. Furthermore, the magnitude of the Doppler shift as a function of wavelength is given by the dispersion relation for gravity wave propagation. Many additional observations of radar echoes from the sea, primarily in the high-frequency (3 to 30 Mhz) portion of the radio-frequency spectrum, have supported this hypothesis. Generally reported features of

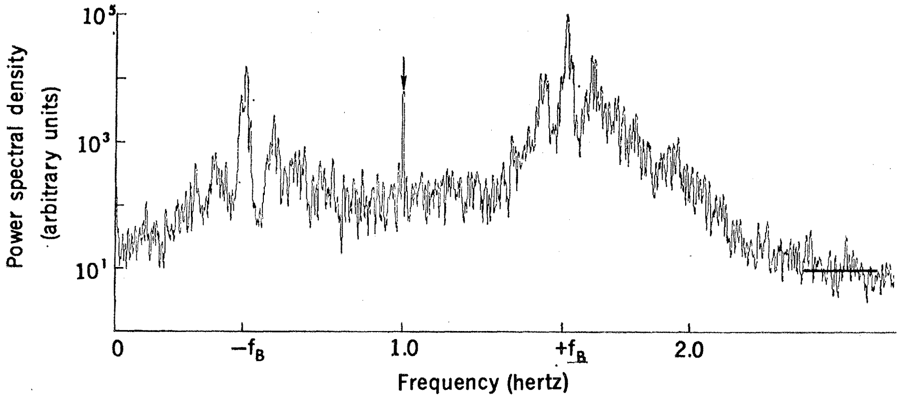

Fig. 1. High-resolution 10.0-m radar echo frequency spectrum obtained on 25 January 1972. The ordinate is the power spectral density of the radar echo from the sea. The line indicated by the arrow is due to reflection from stationary objects. The points indicated by $\pm f_B$ are the theoretical locations of first-order Bragg lines. The spectrum is arranged so that positive Doppler shift is to the right of the stationary line. The bold horizontal line at the right side of the figure is the estimated system noise level.

radar scattering from the sea have been the spectral purity of the echo signal and the consistency of the observed Doppler shifts with the dispersion relation. Obliquely scattered radar returns observed by using well-separated transmitters and receivers are also consistent with first-order Bragg scattering. However, on occasion, additional echo energy has also been observed at frequencies not predicted by the simple Bragg theory. The source of the non-Bragg echoes has remained controversial. In this report we discuss the modifications of the Bragg hypothesis required by second-order scattering mechanisms and present new experimental evidence for the existence of higher-order interactions.

It has been suggested by Hasselmann (*2*) that a Bragg-scattered radar echo, nominally a spectrally pure line, should be accompanied by an echo spectrum continuum resulting from higher-order wave-wave interactions. According to this hypothesis, electromagnetic energy is scattered by those combinations of interacting ocean waves that produce the required $\lambda_e/2$ periodicity on the surface of the sea. Hasselmann bases his analysis on a Feynman diagram formalization of the hydrodynamic effects (*3*), but also includes electromagnetic interaction. In particular, his analysis predicts the presence of symmetrical modulation sidebands on either side of the first-order Bragg line (*2, 3*). These modulation sidebands are predicted to duplicate the wave-height spectrum of the sea. Experimental results obtained by Ward (*4*) have been offered in support of this analysis. The existence of such sidebands would provide an extremely powerful method for remote sensing of the ocean wave spectrum.

A more detailed treatment of the scattering problem, based on Rice's perturbation theory method (*5*), has been carried out by Barrick (*6*), who has obtained an explicit integral representation of the radar echo power spectrum in terms of the directional wave-height spectrum of the sea. Barrick's results are presented in terms of the normalized radar cross section of the sea per radian per second, σ^0. For backscatter from a radio wave propagating in the $\bar{a}_x$ direction, Barrick gives

$$\sigma^0(\eta) = 16\pi k_0^4 \int\int_{-\infty}^{+\infty} |\Gamma(\bar{k}_1, \bar{k}_2)|^2 \times \delta(\eta \pm \omega_1 \pm \omega_2) W(\bar{k}_1) W(\bar{k}_2) dp dq \quad (1)$$

where η is the observed Doppler shift, $\omega - \omega_0$; ω_0 is the frequency of incident electromagnetic waves: k_0 is the free-space wave number; $\delta(\cdot)$ is the Dirac delta function; $W(\cdot)$ is the directional wave-height spectrum of the sea; and $\bar{k}_1$, $\bar{k}_2$, ω_1, and ω_2 are defined by

$$\bar{k}_1 = (p - k_0)\bar{a}_x + q\bar{a}_y$$
$$\bar{k}_2 = -(p + k_0)\bar{a}_x - q\bar{a}_y$$
$$\omega_1 = (g|\bar{k}_1|)^{1/2}, \qquad \omega_2 = (g|\bar{k}_2|)^{1/2}$$

where g is the acceleration due to gravity.

In Eq. 1, the kernel, $\Gamma(\bar{k}_1, \bar{k}_2)$, accounts for both electromagnetic and hydrodynamic wave-wave interactions. The electromagnetic interactions usually correspond to simple multiple scattering from discrete ocean wave components. However, more complex phenomena involving evanescent waves may also occur. Further details may be found in the original paper by Barrick (*6*). In general, the hydrodynamic interactions dominate the process. The evaluation of Eq. 1 by using a semi-isotropic Phillips spectrum (*7*) for $W(\cdot)$ yields continuum sidebands, but they differ significantly from those predicted by Hasselmann (*2*). The representation by Eq. 1 does not predict symmetrical sidebands under general conditions; further, the form of the sidebands, even for an invariant ocean wave spectrum, depends critically on the orientation of the directional wave-height spectrum W to the radio wave propagation direction $\bar{a}_x$.

Figures 1 and 2 present radar echo spectra obtained at a radio wavelength of 10.0 m. The observations were made on the California coast, just south of San Francisco, on 25 and 17 January 1972, respectively. The radar was operated in a coherent pulsed mode with 50-μsec range gates. A directional antenna with a beamwidth of approxi-

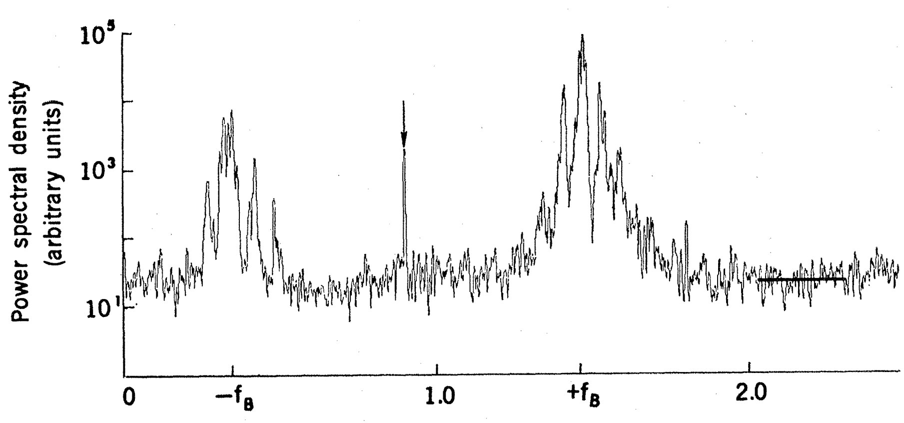

Fig. 2. High-resolution 10.0-m radar echo frequency spectrum obtained on 17 January 1972. The labeling is similar to that of Fig. 1. The nearest sidebands to the $+f_B$ Bragg line correspond to a modulation period of 17 seconds.

mately 60° at one-half power, directed to the west, was employed. The radar was approximately 76 m above the sea so that line-of-sight propagation conditions existed. Each spectrum is the result of about 1000 seconds of observation. The spectra are computed by using digital techniques. Four range intervals, corresponding to a region from about 10 to 40 km from the radar, have been summed to improve the statistics of the spectra. It is of extreme interest that, when examined individually, the echo spectra from these four range intervals are indistinguishable in their primary features. Further smoothing is obtained by taking a running average in frequency over 5-mhz intervals. Unfortunately, the wave-height spectrum of the sea was not available, but when swell was present its period could be estimated from the waves breaking on the beach. In Figs. 1 and 2 the largest echoes correspond to waves moving toward the transmitter. However, negatively shifted Doppler features are always present. In each figure, the approximate noise level of the system is indicated by the bold line to the right of the echoes. The frequency stability of the system is such that the echoes from stationary targets (arrow) were not resolved in frequency, even before the frequency smoothing. In both figures, the first-order Bragg lines themselves show considerable broadening. The points indicated $\pm f_B$ correspond to the theoretical positions of the first-order Bragg lines. It should also be noted that these lines may be shifted significantly, up to about 30 mhz, from their theoretical positions. The causes of this broadening are undetermined; currents along the California coast are of sufficient magnitude to account for the observed shifts.

The spectrum of Fig. 1 is interpreted as arising from a wind-driven sea, in the absence of significant swell. The central feature, indicated by the arrow, is a residual echo from stationary objects and is at the transmitter frequency. Power spectral densities above the system noise level, including the region around the transmitted frequency line, represent scattering from the sea. The spectrum is nonsymmetrical about the Bragg line. We estimate the slope of the spectrum in the region immediately above $+f_B$ to be -40 decibels per hertz; below $+f_B$ the magnitude of positive slope may be twice as great. The overall features of this spectrum are as predicted by Barrick (*6*) and agree quite well with his published theoretical spectra. However, detailed quantitative comparisons, which are quite complex, have not yet been carried out.

Figure 2 is interpreted as arising from a sea surface containing significant long-period components. The frequency displacements of the distinct features in the sidebands about the Bragg lines correspond to modulation with a 17-second period. This period agrees with that of the waves breaking on the beach, as determined with a watch. Modulation sidebands from other swell with a shorter period may also be present. Well-developed, smooth sidebands such as those in Fig. 1 are absent.

These spectra are typical of our observations to date. Significant sideband energy is always present; the nature of the sidebands varies from day to day. In Fig. 1, approximately 50 percent of the total echo signal above the transmitter line is contained in the sidebands. In both figures, the rather well-defined minima on either side of the principal Bragg lines are indicative of a minimum in ocean wave energy at periods of the order of 15 to 20 seconds. We conclude that second-order wave-wave interactions, as first suggested by Hasselmann (*2*), do occur and that they are observable. The more detailed calculations of Barrick (*6*) account for the observed features of the spectra. From the variation of the sidebands with time over a period of 1 day, we conclude that these sidebands are quite sensitive to the total wave-height spectrum of the ocean, as has been suggested. Consequently, it seems likely that decameter radar will be able to provide measurements of the sea state. This has not previously been possible because of the technical difficulties of carrying out observations with the frequency resolution and dynamic range of those described here.

G. LEONARD TYLER
WILLIAM E. FAULKERSON
ALLEN M. PETERSON
CALVIN C. TEAGUE
Center for Radar Astronomy, Stanford University, Stanford, California 94305

References and Notes

1. D. D. Crombie, *Nature* **175**, 681 (1955).
2. K. Hasselmann, *Nature Phys. Sci.* **229**, 16 (1971).
3. ———, *Rev. Geophys.* **4**, 1 (1966).
4. J. F. Ward, *Nature* **223**, 1325 (1969).
5. S. O. Rice, *Commun. Pure Appl. Math.* **4**, 351 (1951).
6. D. E. Barrick, in *Remote Sensing of the Troposphere*, V. Derr, Ed. (Government Printing Office, Washington, D.C., 1972), chap. 12.
7. O. M. Phillips, *The Dynamics of the Upper Ocean* (Cambridge Univ. Press, London, 1966).
8. This work was carried out at the Stanford Center for Radar Astronomy as part of a joint study with Scripps Institute of Oceanography. Financial support for this work is provided by Scripps Institute of Oceanography under ARPA contract N00014-69-A-0200-6012.

17 April 1972; revised 7 June 1972

Sea Level at Southern California: A Decadal Fluctuation

Abstract. *The winter mean height of sea level at southern California rose 5.6 centimeters between the periods 1948–1957 and 1958–1969. These periods correspond to two fairly coherent large-scale climatic regimes with different air-sea coupling, which were previously identified. The rise was mainly due to a change in the thermohaline structure of the water as a result of changes in prevailing winds.*

Winters in the decade of the 1960's were anomalously cold over the eastern United States but warmer than normal over the Far West (*1*). This short-period climatic fluctuation was attributed to an amplified atmospheric long-wave pattern in which a strong trough (equatorward bulge in the upper westerlies) dominated the central Pacific. The downstream response to this feature was a strong ridge in western North America and a strong trough in the East. Subsequently, Komhyr *et al.* (*2*) related observed increases in total ozone during the 1960's to this anomalous pattern. It was suggested (*1*) that this anomalous circulation pattern may have been forced by anomalous temperatures at the surface of the sea in the North Pacific.

Further studies of this regime (*3*) and the regime of the preceding decade indicate that an abrupt transition occurred in about 1957–1958 between radically different winter patterns of atmospheric circulation and temperature. An example of this break between two coherent regimes is the winter temperature in Atlanta, Georgia, which averaged 3°C colder in the later period than in the earlier.

Because of the large winter differences in mean pressure gradient and sea surface temperature off the West Coast in these roughly decadal periods, as shown in Fig. 1, we considered a